Potential for estimating cloud liquid water path over sea ice from airborne passive microwave measurements

Julie A. Haggerty[1] and Judith A. Curry
Program in Atmospheric and Oceanic Sciences, University of Colorado, Boulder, Colorado, USA

Guosheng Liu
Department of Meteorology, Florida State University, Tallahassee, Florida, USA

Received 2 March 2001; revised 9 July 2001; accepted 13 July 2001; published 9 January 2002.

[1] In this paper we investigate the feasibility of determining cloud liquid water path from passive microwave measurements over sea ice. Simulations using a 32-stream plane-parallel microwave radiative transfer model indicate a consistent increase in brightness temperature attributable to cloud liquid water for conditions observed in the Arctic during the Surface Heat Budget of the Arctic (SHEBA) experiment. Uncertainties in brightness temperature simulations due to variations in surface emissivity, surface temperature, cloud temperature, and atmospheric water vapor are investigated. Surface emissivity variations are found to cause the largest uncertainties in top-of-atmosphere brightness temperature over the range of liquid water paths examined. An algorithm previously developed for estimating liquid water path over oceans from SSM/I data is adapted for retrievals over sea ice. The algorithm is applied to brightness temperature measurements from airborne microwave radiometers. Mean retrieved liquid water path (LWP) is compared to in situ measurements from airborne cloud microphysical probes. The correlation coefficient for the two data sets is found to be 0.989 with an RMS error of 14 g m^{-2}, although the retrieved LWP values show a high degree of variability. Accuracy is highest when LWP values are 100 g m^{-2} and above. Poorest accuracies are obtained for small LWP (<50 g m^{-2}) where errors in the specification of surface emissivity have a large effect. These case studies provide evidence that liquid water clouds over sea ice produce detectable changes in microwave brightness temperature and suggest that interpretation of sea ice properties using certain microwave frequencies may be affected by the presence of liquid water clouds. *INDEX TERMS:* 0320 Atmospheric Composition and Structure: Cloud physics and chemistry, 3349 Meteorology and Atmospheric Dynamics: Polar meteorology, 3360 Meteorology and Atmospheric Dynamics: Remote sensing, 3394 Meteorology and Atmospheric Dynamics: Instruments and techniques; *KEYWORDS:* cloud physics, microwave remote sensing, arctic clouds, liquid water path, airborne measurements

1. Introduction

[2] Climate modeling results have indicated the vulnerability of the Arctic to global climate change [e.g., *Washington and Meehl*, 1989]. Potential effects of global warming on the polar sea ice have heightened interest in understanding the factors that control polar atmospheric, oceanic, and ice processes. Expanding our knowledge of cloud processes, particularly in the data-sparse Arctic region, is important for improving model predictions. Cloud microphysical and macrophysical properties have a critical influence on radiative fluxes [*Curry et al.*, 1993; *Francis*, 1999]. Changes in cloud properties have been hypothesized by *Curry et al.* [1993] to have a significant impact on the sea ice mass balance. The selection of a cloud parameterization scheme can cause large discrepancies in climate simulations [*Browning*, 1994]. On an operational level, cloud cover may produce spurious results in sea ice concentration estimates [*Cavalieri et al.*, 1999].

[3] Despite the need for understanding the complexities of Arctic cloud processes, little observational cloud data are available. Satellite retrieval techniques, which provide information about clouds over other remote areas of the world, encounter difficulties in polar regions due to the fact that Arctic clouds are frequently low level and optically thin [*Curry et al.*, 1996]. Given the high albedo of the snow/ice surface, there is little contrast between clouds and surface in the visible part of the spectrum. Since the clouds are low, their temperatures tend to be close to that of the surface, so there is little thermal contrast as well [*Key and Barry*, 1990]. Microwave emissivities of the sea ice surface are high and variable, so Arctic clouds containing small amounts of liquid or ice water do not have a large effect on the microwave signal, especially at lower frequencies. To further investigate the potential for improving remote sensing methods in the Arctic, aircraft observations were conducted as part of the FIRE Arctic Clouds Experiment (FIRE ACE) in conjunction with the Surface Heat Budget of the Arctic (SHEBA) experiment [*Curry et al.*, 2000; *Perovich et al.*, 1999a].

[4] Passive microwave measurements from satellites have been used in other parts of the world to estimate cloud properties such as liquid water path, ice water path, and precipitation rate. Most retrievals are performed over ocean surfaces where the low, uniform surface emissivity provides significant contrast with overlying clouds [e.g., *Liu and Curry*, 1993; *Kummerow et al.*, 1996]. Liquid water path (LWP) retrievals over land have also been attempted, using passive microwave data [*Greenwald et al.*, 1997]. Cloud retrievals over sea ice encounter similar challenges as those over land, namely the separation of the cloud signal from emission by a radiometrically warm surface that may experience frequent changes

[1] Now at National Center for Atmospheric Research, Boulder, Colorado, USA.

0148-0227/02/2001JD000585$09.00

in its dielectric properties. Thus there have been no attempts, to date, to relate cloud liquid or ice water path to satellite microwave radiances over sea ice. Model simulation studies suggest, however, that in some circumstances the cloud LWP signal is significant at frequencies of 85–90 GHz and is discernible against the bright sea ice background (G. Liu and J. Curry, Observation and interpretation of microwave hot spots over the Arctic Ocean during winter, submitted to *Journal of Geophysical Research*, 2001).

[5] Visual evidence from sequential images of Special Sensor Microwave Imager (SSM/I) 85 GHz images confirms the detectability of clouds over sea ice. In fact, it has been shown that emissivities of multiyear sea ice at frequencies of 85 GHz and higher may be as low as emissivities of seawater at the same frequencies [*Hollinger et al.*, 1984; *English and Hewison*, 1998]. Theoretical studies [*English*, 1999] and attempted LWP retrievals over land [*Jones and Vonder Haar*, 1990; *Greenwald et al.*, 1997; *Combs et al.*, 1998] suggest that there is potential for retrieving cloud LWP over land and sea ice but that results are very sensitive to the specification of surface emissivity and other parameters.

[6] In this study we examine the feasibility of retrieving cloud LWP over sea ice using measurements from SHEBA and FIRE ACE. Specifically, we address the following questions:

1. Which of the available microwave frequencies are best suited for LWP retrievals over sea ice?
2. What are the effects of uncertainties in surface emissivity and other parameters on LWP retrievals?
3. Which types of surface conditions are optimal for performing LWP retrievals?
4. What levels of LWP are detectable and how accurate are the retrievals?
5. How common are detectable levels of LWP throughout an annual cycle in the Arctic?

[7] In the remainder of the paper we describe data used for this study (section 2), discuss model simulations of microwave brightness temperatures under various conditions (section 3), explain methods used for LWP retrieval and validation (section 4), and present results from several LWP retrieval attempts (section 5).

2. Data Sets

2.1. Field Experiment

[8] The Surface Heat Budget of the Arctic (SHEBA) experiment was conducted from October 1997 to October 1998 in the Beaufort and Chukchi Seas [*Perovich et al.*, 1999a]. The Canadian Coast Guard icebreaker *Des Groseilliers* served as a base camp to deploy a variety of sensors to measure ice, snow, and meteorological properties. In conjunction with the SHEBA effort, the FIRE Arctic Clouds Experiment (FIRE ACE) extended the spatial domain of SHEBA with aircraft observations of atmospheric and surface properties near the *Des Groseilliers* [*Curry et al.*, 2000]. Aircraft measurements in the vicinity of the SHEBA ice station were conducted in the spring and summer of 1998. Of particular interest for this work are flights by the National Center for Atmospheric Research (NCAR) C-130 aircraft, which operated at altitudes between 100 m and 7000 m, and the NASA ER-2 aircraft, which operated at altitudes of ~20 km. The payload on each aircraft included a scanning microwave radiometer system, while the NCAR C-130 also carried in situ sensors useful for validation purposes.

2.2. Instrumentation

[9] The Airborne Imaging Microwave Radiometer (AIMR) is a cross-track scanning system which flies on the NCAR C-130. Four channels measure upwelling radiation at two frequencies, 37 and 90 GHz, and two orthogonal polarizations that can be converted to horizontal and vertical components. The AIMR views underlying scenes over an angular swath of 120°. Beam widths of 1° at 90 GHz and 2.8° at 37 GHz produce spatial resolutions on the order of 20–300 m at typical flight altitudes and velocities. Corresponding swath widths are ~3–20 km. Calibration is performed internally as the scanning mirror views heated and ambient temperature loads following observation of the scene radiances. Estimated errors are on the order of 1–2 K for brightness temperatures between 150 K and 350 K. Detailed specifications for the AIMR can be found in the work of *Collins et al.* [1996].

[10] The Millimeter Imaging Radiometer (MIR) was flown on the NASA ER-2 during FIRE SHEBA. The MIR is a cross-track scanner measuring microwave radiation at several frequencies, including 89, 150, and 220 GHz. It scans over an angular swath of 100° and has a 3.5° beam width. Resulting swath width at the typical 20 km flight altitude of the ER-2 is ~48 km. The MIR calibration system is similar to that of AIMR with two internal loads viewed during each scan. *Racette et al.* [1996] give error estimates of better than 1 K for brightness temperatures between 240 K and 300 K. Postflight calibration efforts have demonstrated errors on the order of 2–4 K for brightness temperatures below 100 K. Separation of the vertically and horizontally polarized components is not possible with this instrument, so mixtures of brightness temperature components are used for calculations of emissivity.

[11] Results from the passive microwave retrievals of LWP are compared to vertically integrated liquid water content (LWC) measurements from airborne in situ sensors. These sensors provide an independent measure of cloud liquid water very close in space and time to the retrieved estimate. The King hot wire probe relates cloud liquid water content to the amount of heat generated when water droplets are vaporized, providing measurements over a range of 0.05–3.0 g m^{-3} [*National Center for Atmospheric Reasearch* (*NCAR*), 1994]. Its accuracy is estimated to be on the order of 15%, but errors are thought to be significantly greater when water droplets are larger than 40 μm in diameter. Liquid water content is also measured by a Gerber particle volume monitor-100 (PVM-100) [*Gerber et al.*, 1994]. Following correction of a bias in the King probe measurements [K. Laursen, personal communication, 2000], agreement between the PVM-100 and the King probes is very good.

[12] Surface (skin) temperatures are measured remotely from below-cloud flight segments using a set of two Heimann model KT19.85 pyrometers [*NCAR*, 1994]. The Heimann radiometers detect radiation within the spectral range 9.6–1.5 μm over a 2° field of view. The sensors cover a measurement range from −50°C to +60°C with a resolution of 0.005°C. Absolute accuracy is ±0.5°C plus 0.7% of the difference between the sensor housing temperature and the scene temperature. During FIRE SHEBA, the sensor was maintained at 286–290 K, while the coldest scene temperatures observed were on the order of 257 K. In the worst case, the specified error is then 0.73 K.

2.3. Overview of Cloud Conditions During FIRE SHEBA

[13] Cloud radar and lidar systems based at the SHEBA site observed cloud conditions over an annual cycle. Analyses of these data by *Intrieri et al.* [2001] show that clouds were present 85% of the time with maximum cloudiness in summer and minimum in winter. Lidar observations demonstrate that liquid water was present in clouds throughout the year, even in the coldest winter months. Liquid water was observed in nearly three fourths of the observed clouds. Cloud base heights were found to be variable throughout the year with monthly averages between 450 m and 1850 m. Monthly averaged cloud top heights ranged from 2800 to 5500 m. Multiple cloud layers were commonly detected.

[14] Aircraft campaigns were conducted in spring and summer [*Curry et al.*, 2000]. Cloud observations from those platforms reveal a persistent cloud-topped surface mixed layer during the first 3 in May followed by a period of clear skies. Clouds were generally mixed phase in the first half of May and liquid phase later in the month. Multilayered clouds were common in June with appreciable variation in base and top heights over short distances.

Storms in July brought frequent middle- and high-level clouds. Periodic surface fog was also observed. Clouds with all liquid, all ice, and mixed-phase particles were observed during July. Observed cloud temperatures in both liquid and mixed-phase clouds were nearly always below freezing [*Jensen and Lawson*, 1999].

3. Model Simulations

[15] To understand the response of AIMR and MIR measurements in an Arctic environment, numerical simulations of top-of-atmosphere (TOA) brightness temperatures (T_B) were conducted for conditions approximating those observed during spring and summer around the SHEBA site. The plane-parallel microwave radiative transfer model [*Liu*, 1998] calculates absorption coefficients for atmospheric gases (water vapor and oxygen) according to *Liebe and Layton* [1987]. Comparisons with a newer model for gaseous absorption [*Rosenkranz*, 1998] showed small differences (less than 0.5 K) between the two models for Arctic conditions. Absorption and scattering coefficients and phase functions for condensed water and ice are calculated using Mie theory. The complex refractive indices of liquid water are taken from the empirical formulations of *Ray* [1972]. Refractive indices for ice are from *Warren* [1984]. As noted by *Lin et al.* [1998], there are no measurements to support the liquid water parameterizations at cloud temperatures below 258 K. Significant disagreement exists between the Ray parameterizations and the *Liebe et al.* [1991] parameterizations for supercooled water, as demonstrated by *Lipton et al.* [1999]. Given the insufficient number of measurements to support a specific parameterization at supercooled temperatures, we use the Ray parameterizations following *Liu and Curry* [1993] and *Lin et al.* [1998].

[16] A series of baseline cases representing observed conditions during FIRE SHEBA has been defined for these simulations. Temperature and water vapor profiles from aircraft measurements are used up to flight levels of about 6 km. Above this level, standard profiles representing summer subarctic conditions are blended with the measured profiles. Cloud heights and temperatures are also derived from the aircraft profiles. Surface emissivity values are based on estimates from *Haggerty and Curry* [2001]. Surface temperatures are estimated from aircraft infrared radiometer measurements.

[17] Initial model runs focus on nonprecipitating liquid phase clouds with droplet radii smaller than 100 um. The effects of scattering by cloud ice are considered in the next section, although it is known that absorption by liquid is the dominant extinction mechanism at these frequencies [*Ulaby et al.*, 1981]. Liquid water path is varied over a range suggested by in situ aircraft measurements of liquid water content and ground-based measurements from a 31 GHz microwave radiometer [*Han et al.*, 2001; *Lin et al.*, 2001]. On the basis of these measurements we vary LWP over a range of 0–200 g m^{-2} in May and 0–500 g m^{-2} in July.

[18] Four cases are assembled to represent the range of conditions seen during FIRE SHEBA in May and July. The properties of each case are listed in Table 1. The cases comprise a range of cloud heights, temperature, and humidity as measured during aircraft slant path profiles. To simplify the interpretation of the effect of cloud temperature on TOA brightness temperatures, cloud layers within each profile are assumed isothermal. Cloud temperatures are below freezing in May and near freezing and above in July. Clouds are assumed to contain no ice particles for the initial simulations. Assumed surface emissivities are given in Table 2. May values are representative of a dry snow layer covering the multiyear ice. Low emissivity values at 90 and 150 GHz are found to result from volume scattering by the snow layer. Melting conditions in July raise the emissivity at 90 GHz. Simulations are performed for horizontal polarizations at 37 and 90 GHz, since the lower emissivity at high viewing angles should provide better contrast between surface and atmosphere. Note that MIR data are not available in July, so only AIMR frequencies (37 and 90 GHz) are considered in the July simulations.

Table 1. Specifications for MWRT Simulations

Date (Case)	Surface Temperature, K	Cloud		Precipitable Water, kg m^{-2}
		Height, m	Temperature, K	
May 15 (a)	264.1	100–400	264.8	5.8
May 27 (b)	272.2	100–500	270.6	12.6
		1300–1500	271.9	
July 18 (c)	273.2	0–100	276.2	22.7
		2000–3500	269.5	
July 29 (d)	273.2	100–500	270.5	12.2

Table 2. Surface Emissivity Values at 53° for MWRT Simulations

Case	H pol			
	37 GHz	90 GHz	150 GHz	220 GHz
a, b (May)	0.84	0.68	0.72	0.84
c, d (July)	0.83	0.80	–	–

3.1. Brightness Temperature Variations

[19] Results are presented in Figure 1, which shows T_B as a function of LWP for each case. In all cases we see an increase in T_B over the range of LWP considered. The magnitude of the changes, however, varies substantially between frequencies. In Figure 1a the effect of increasing LWP is largest at 90 and 150 GHz with ΔT_B of 27–29 K. A higher surface emission term coupled with lower liquid water emission at 37 GHz produces little change at that frequency in these conditions. The T_B variation is also small at 220 GHz where the surface emission is higher and atmospheric water vapor emission is larger than at the lower frequencies. Variations are similar in Figure 1b, although higher surface temperature and atmospheric water vapor burden raise the baseline (no liquid water) value of T_B at all frequencies. Note that the average cloud temperature in this case (264 K) raises questions about the accuracy of the model's liquid water parameterization [*Lin et al.*, 2001; *Lipton et al.*, 1999].

[20] The resulting ΔT_B values at both 90 and 150 GHz are lower in Figure 1b due to higher background T_B. The higher cloud temperatures compared to Figure 1a may also contribute to the reduced LWP signal. The absorption coefficient of liquid water decreases with increasing temperature [*Ulaby et al.*, 1986], so the emissivity of a warmer cloud is lower than that of a colder cloud (although the variation for supercooled water has not been documented). The higher emitting temperature of the cloud serves to increase the total emission, however, so this effect offsets the reduction in cloud emissivity. In this case, it is not clear which effect is dominant.

[21] The summertime cases also exhibit steady increases in T_B with increasing LWP. Surface conditions at this time tend to reduce the contrast between surface radiation and atmospheric radiation. Emissivity is higher for melting ice and snow, and surface temperatures are significantly warmer. Higher water vapor levels, as seen in case c (Table 1), also contribute to higher background T_B values. Therefore in Figures 1c and 1d, we see 90 GHz ΔT_B on the order of 15 and 20 K, respectively, for a change in liquid water path of 500 g m^{-2}.

[22] On the basis of this analysis it appears that the 90 GHz (horizontal) signal contains the most information about LWP values in the conditions encountered during FIRE SHEBA. Conditions for which liquid water produces the largest ΔT_B are those with lower surface emission, i.e., low physical temperatures and/or

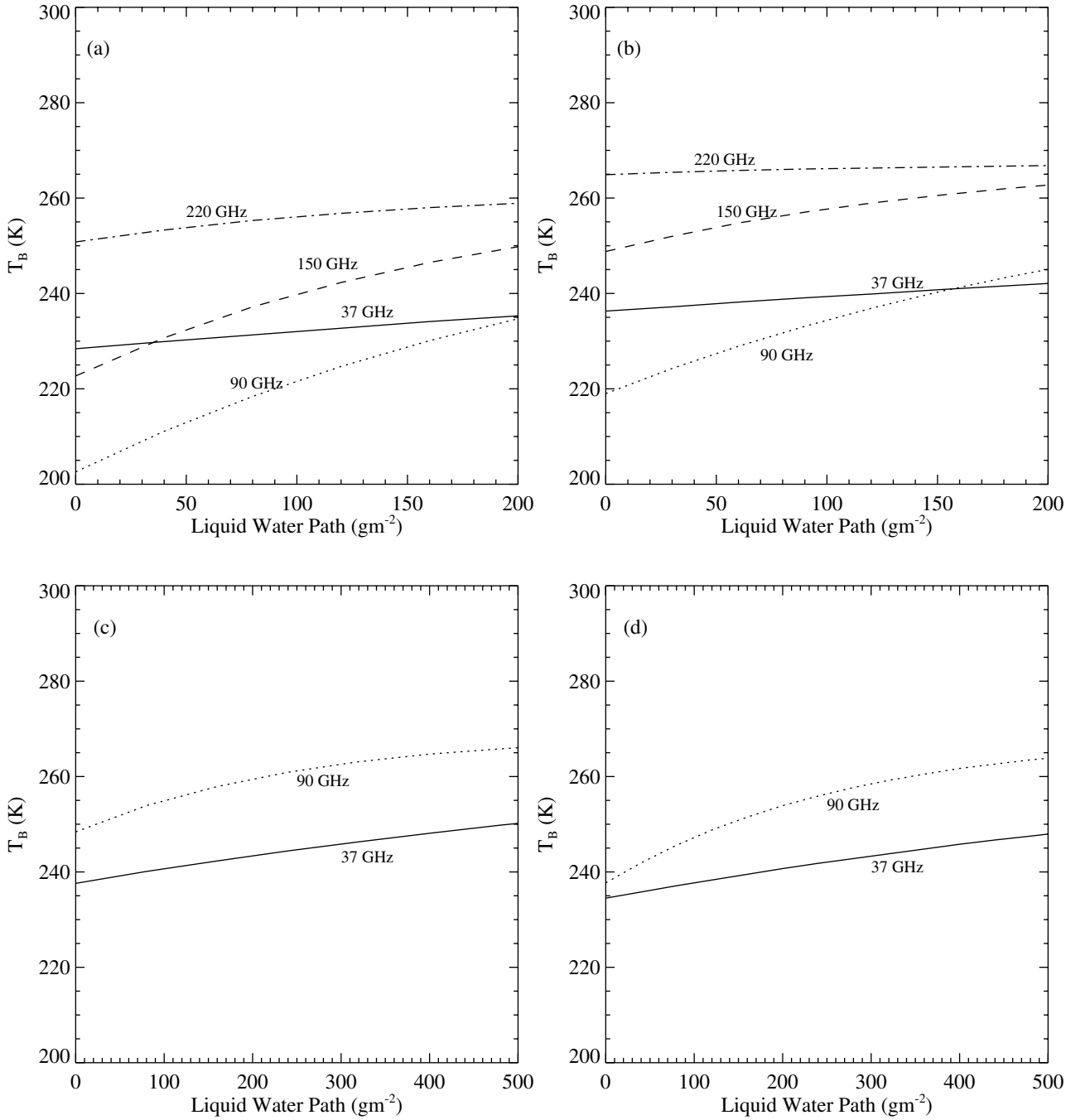

Figure 1. Model-simulated brightness temperatures for cases a–d as described in Tables 1 and 2.

low emissivity. Emissivity at 90 GHz tends to be lower for dry snow due to volume scattering [*Grody*, 1993] and higher for summer melt conditions [*Eppler et al.*, 1992]. Physical temperatures warm as summer approaches. Therefore it would appear that springtime (snow covered) conditions provide a better opportunity for accurate estimations of liquid water path. Higher LWP values in the summer may compensate for the reduction in contrast due to higher surface emission.

3.2. Sensitivity Analysis

[23] Given that Arctic conditions generally consist of relatively low LWP values coupled with fairly high surface emissivity, the magnitude of ΔT_B is small compared to that seen in other parts of the world (e.g., over the ocean). Uncertainties in other atmospheric and surface variables may produce ΔT_B values that are significant compared to those produced by LWP changes in the Arctic. In this section we examine the effect on ΔT_B of uncertainties in surface emissivity, surface temperature, atmospheric water vapor, cloud temperature, and cloud ice.

3.2.1. Surface properties. [24] Microwave surface emissivities of snow and sea ice are difficult to estimate and may also be quite variable in time and space. For this analysis we begin with the values estimated at SHEBA [*Haggerty and Curry*, 2001] and vary the emissivity (ε_s) by one standard deviation as calculated over a 50 × 50 km box around the SHEBA site. In May, $\Delta\varepsilon_s$ is assigned a value ±0.05, and in July, $\Delta\varepsilon_s$ is ±0.03. Note that these

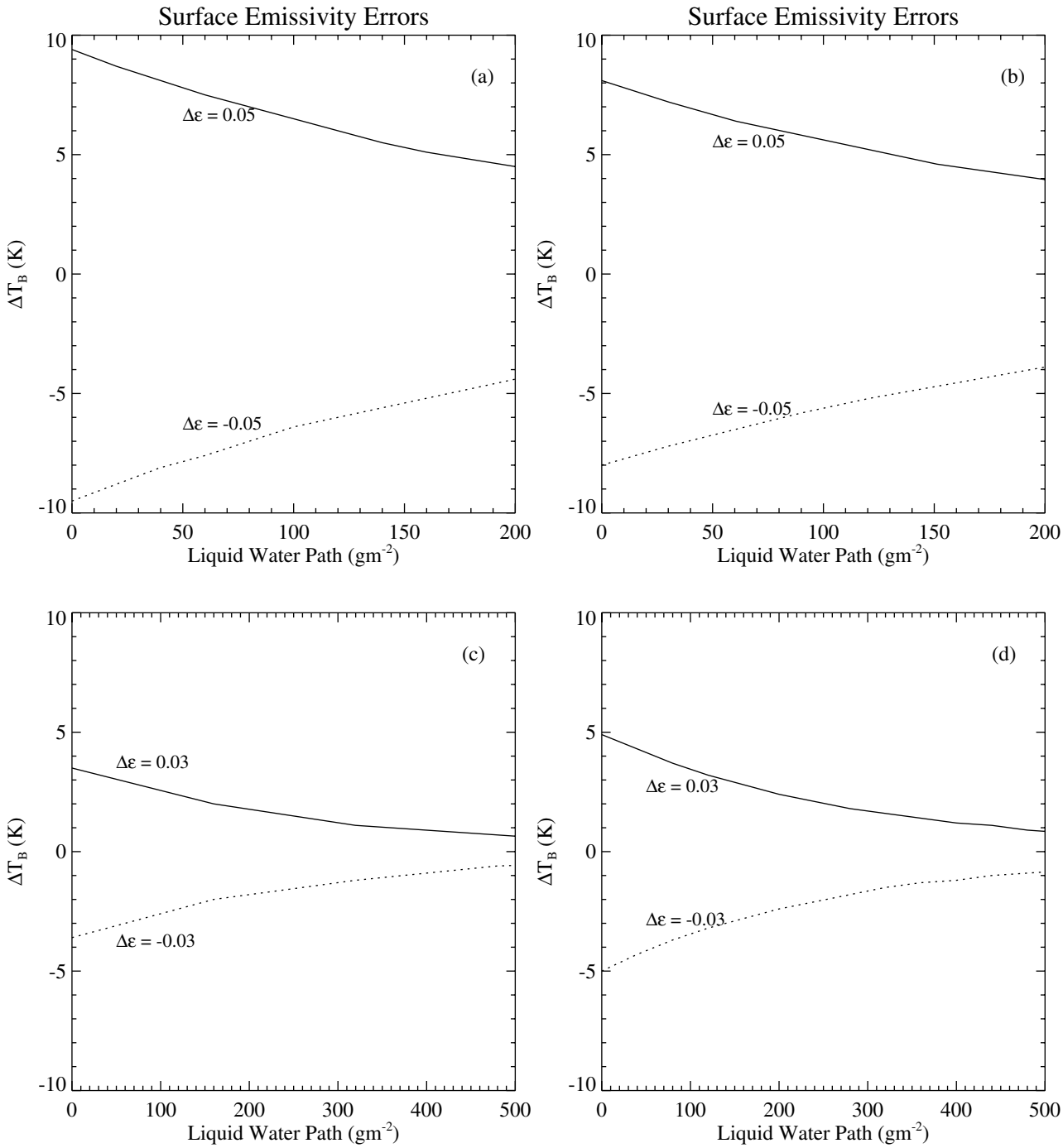

Figure 2. Effect of errors in surface emissivity on simulated brightness temperatures at 90 GHz for cases a–d as described in Tables 1 and 2.

estimates characterize variations documented within the multiyear ice pack. New ice and open water in leads, which often exhibit larger $\Delta\varepsilon_s$, are excluded from the estimates. The magnitudes of these variations are consistent with variations given by *Eppler et al.* [1992]. We perform the sensitivity analyses at 90 GHz for all cases since that frequency exhibited the largest T_B variations over the range of LWP values simulated.

[25] Figure 2 shows the effects of surface emissivity uncertainties on ΔT_B at 90 GHz for the four cases. At the low LWP values typically observed in spring (<100 gm^{-2}), ΔT_B due to emissivity uncertainties is on the order of 6–9 K. This variation is a significant amount of the LWP-induced T_B variation of 25–30 K, demonstrating the importance of accurate surface emissivity estimates. The effect is smaller in summer (Figures 2c and 2d) due to smaller emissivity variations and masking by higher atmospheric water content (vapor and liquid). We note that the $\Delta\varepsilon_s$ values used here are representative of the variation encountered over a fairly uniform snow or ice surface. In situations where more than one surface type is present, or the wrong surface type is assumed (e.g., new ice versus multiyear ice), $\Delta\varepsilon_s$ could potentially be much larger.

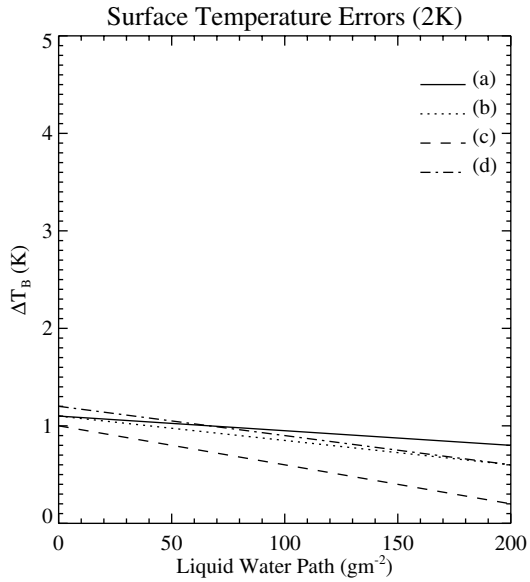

Figure 3. Effect of a 2 K error in surface temperature on simulated brightness temperatures at 90 GHz for cases a–d as described in Tables 1 and 2.

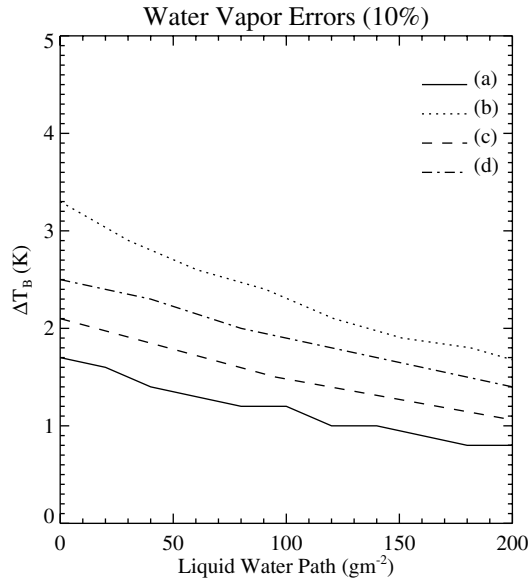

Figure 4. Effect of a 10% error in relative humidity on simulated brightness temperatures at 90 GHz for cases a–d as described in Tables 1 and 2.

[26] Surface (skin) temperature uncertainties are shown to be relatively small [Haggerty et al., 2001]. Standard deviations over the area are less than 0.5 K in May and July (excluding leads). Since microwave surface emission emanates from a layer that may be several centimeters thick, the skin temperature variation may not be a good representation of the total uncertainty. Thus we use a ΔT_s value of 2 K for our analysis. Results for each of the four cases are shown in Figure 3. The effect of ΔT_B at 90 GHz is on the order of 1 K or less and decreases with increasing LWP. It is evident that surface temperature uncertainties are far less significant than surface emissivity errors.

3.2.2. Atmospheric properties. [27] The effects of uncertainty in atmospheric water vapor are considered by adding 10% to relative humidity throughout the profile (equivalent to a change in precipitable water of 2–3 kg m^{-2} for cases considered here). Figure 4 shows the resulting ΔT_B as a function of LWP. At low LWP values, ΔT_B is on the order of 2–3 K, but it decreases to about 1 K as LWP increases. Similarly, we evaluate the effect of uncertainty in cloud temperature by introducing changes of ±2 K throughout the cloud layers. Effects of cloud temperature uncertainties are smaller by an order of magnitude than uncertainties in surface properties and relative humidity for cases a, b, and d where the clouds are relatively thin. Differences due to cloud temperature uncertainties for case c are shown in Figure 5. Here temperature changes over a cloud layer 1500 m thick produce ΔT_B on the order of 1 K. We note that T_B is higher when cloud temperature is higher and lower when cloud temperature is lower, suggesting that the effect of emitting temperature outweighs the opposing effect of temperature changes on cloud emissivity. The effects of multiple cloud layers on ΔT_B are also examined with modifications to case c. A third cloud layer with a temperature of 259 K is placed at 4500–5000 m. Other specifications remain the same. The absorption and reradiation of surface and lower cloud layer emissions by the higher (colder) cloud have little effect on the result. The difference in T_B is less than 1.5 K over the LWP range simulated.

[28] Finally, we examine the effects of cloud ice particles on the TOA brightness temperature. Cloud radar retrievals at the SHEBA site estimate mean ice particle diameters of 55 μm during the period April–July 1998 [*Shupe et al.*, 2001]. Corresponding mean ice water contents are on the order of 0.005 g m^{-3}. Few estimates of ice water path during SHEBA are currently available, but a July case, analyzed by *Khvorostyanov et al.* [2001], finds IWP of about 75 g m^{-2} based on in situ aircraft measurements and radar retrievals in altostratus and cirrus cloud layers overlying the SHEBA site. Using the available ice property estimates, we modify the simulations in cases a and c to include nonprecipitating cloud ice particles. In both cases the cloud temperatures are below freezing and in situ observations [*Jensen and Lawson*, 1999] reveal mixed-phase clouds. We assume an ice water path (IWP) of 80 g m^{-2} distributed throughout the single cloud layer in case a and the upper cloud layer in case c and a mean particle diameter of 50 μm. Ice density is assumed to be 0.3 g cm^{-3}. Because of lack of information about particle shape, ice particles are assumed spher-

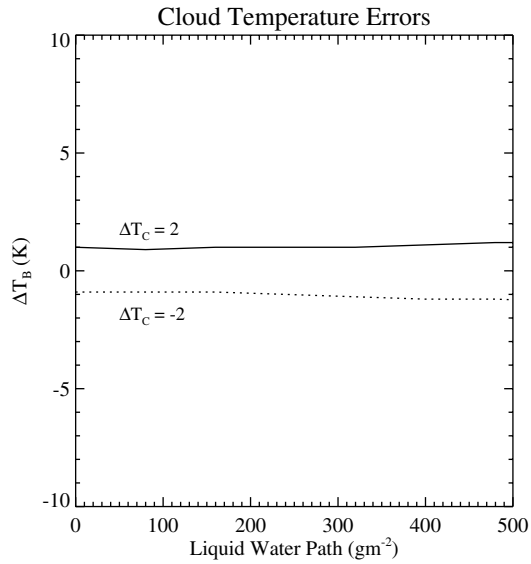

Figure 5. Effect of errors in cloud temperature on simulated brightness temperatures at 90 GHz for case c as described in Tables 1 and 2.

ical, although *Evans and Stephens* [1995] have shown that the effect of shape on scattering can be significant. Results show no discernible effect of the ice at 37 GHz, and ΔT_B at 90 GHz shows a depression of about 0.1 K at all LWP values. Even at 150 and 220 GHz, the depression in T_B due to scattering is not large ($\sim$1–2 K). These results suggest that for the average conditions observed during spring and summer in SHEBA, nonprecipitating ice particles do not have a significant effect on T_B at 90 GHz.

[29] Larger (precipitation size) ice particles were occasionally observed during the FIRE-SHEBA flights. For example, ice particle diameters observed on July 29 varied from 200 to 2000 μm. We simulate the effect of precipitation using size distributions defined by *Liu and Curry* [1998]. Ice water path is assumed to vary from zero to 200 g m^{-2} based on IWP retrievals described by *Wang et al.* [2001]. Ice density is assumed to be 0.3 g cm^{-3}, and ice particles are assumed to be spherical. A 500-m-deep ice cloud is placed at 4500 m in case d, which is consistent with observations during part of that day. Results show that at these IWP values the T_B depression at 90 GHz, due to scattering by precipitation size ice particles, is as much as 15–20 K. Clearly, the presence of large ice particles could have a significant effect on LWP retrievals.

4. LWP Estimation

4.1. Retrieval Method

[30] The physical principles governing microwave transfer through liquid hydrometeors have been studied extensively, and numerous statistically and physically based methods for estimating LWP have been developed. Statistical methods [e.g., *Weng and Grody*, 1994] generally require a substantial set of "training data" to develop coefficients appropriate for the conditions encountered. Given that the Arctic is a data-sparse region in general, it is unlikely that a sufficient data set would be available to successfully perform statistical retrievals. For this reason we concentrate on physical retrieval methods [e.g., *Liu and Curry*, 1993; *Westwater*, 1993; *Lin et al.*, 1998]. Furthermore, some methods estimate other variables simultaneously with LWP (e.g., cloud temperature or water vapor amount). Since the FIRE-ACE data set includes ancillary measurements of such variables, we opt to use a method that estimates LWP exclusively. In this way we limit the complexity of the problem allowing us to more easily isolate and understand sources of uncertainty in the retrievals.

[31] We begin with the physically based method of *Liu and Curry* [1993], which has previously been used to derive LWP from SSM/I data over ocean. It is shown that LWP can be obtained from

$$LWP = \frac{1}{\Omega} \log\left(\frac{1}{1-\varepsilon_c}\right) \cos\theta\,, \tag{1}$$

where Ω is the liquid water absorption coefficient and a function of frequency and cloud mean temperature, ε_c is the cloud emissivity, and θ is the viewing angle. Cloud emissivity is derived from a quadratic equation, which depends on five temperatures: T_B, the brightness temperature of a cloudy scene at a given frequency; T_{B0}, the corresponding clear-sky brightness temperature which accounts for emission from the surface and atmospheric water vapor; T_C, the cloud mean temperature; T_A, the mean air temperature; and T_s, the surface temperature. The Liu and Curry method has been previously adapted for use with a scanning airborne radiometer [*Haggerty*, 2001].

[32] In our implementation of this algorithm, T_A, and T_C are obtained from aircraft profiles through the observed cloud layer. T_s is measured by the Heimann radiometers during below-cloud flight segments, and T_B is measured by the microwave radiometers. T_{B0} is constructed using the *Liu* [1998] microwave radiative transfer model with input from aircraft temperature and humidity profiles, surface temperature, and surface emissivity. Retrievals are performed at 90 GHz (horizontal polarization) on the basis of results of model simulations.

[33] As demonstrated in section 3, retrievals are quite sensitive to the value of surface emissivity used for T_{B0} estimates. We perform initial calculations of T_{B0} using estimates of mean surface emissivity from clear-sky days. We assume that ε_s is uniform over the observation area of 50 × 50 km centered on the SHEBA site. Variations in ε_s tend to be large in leads that may contain combinations of various ice types and open water. For this reason, lead surface emissivities are not well represented by a mean ε_s, so we have elected to exclude lead pixels from our LWP retrievals. Detection of leads is straightforward since T_B values in leads tend to be subtantially higher (lower) than the surrounding multiyear ice in spring (summer). In some cases, clouds are thick enough to mask surface variations, so leads are not easily detectable. In this situation, however, the surface emission term is not so significant as it is for thinner cloud conditions, so including leads should not degrade the accuracy of the retrieval.

[34] The use of a uniform ε_s derived from clear-sky days introduces error even when only multiyear ice surfaces are included. We have already examined the effect of spatial variations in ε_s on a given day (section 3), but temporal variations between flight days may also be significant. Changes in surface conditions due to melting, freezing, or precipitation can produce large changes in ε_s. During the time periods examined here (May and July 1998), bulk surface conditions (exclusive of leads) remained relatively constant. In May, surface observers reported dry snow of fairly constant depth until late in the month when melting began [*Perovich et al.*, 1999b]. Throughout July, surface temperatures remained near the freezing point and significant amounts of liquid were observed on the surface. Late in the month, the surface temperature dropped slightly below freezing and observers reported new ice formation. During that time, precipitation associated with a frontal passage may have also contributed to ε_s changes. A priori knowledge of a possible change in the surface dielectric properties suggests that the mean ε_s value from the nearest in time clear-sky day may not be a good estimate. In such cases we attempt to find below-cloud flight segments on a given day and calculate a more representative value of ε_s.

4.2. Validation Method

[35] Liquid water contents (LWCs) from the King hot wire and Gerber PVM-100 probes are integrated through the cloud layer to obtain an in situ measurement of LWP for comparison with retrievals. Given the small-scale inhomogeneities that may occur in the spatial distribution of cloud liquid water, a single estimate of LWP obtained from an aircraft slant profile cannot represent the array of values derived from a two-dimensional image, but aircraft measurements provide some indication of the accuracy of the algorithm.

[36] During the course of a C-130 flight the aircraft typically flew a series of 50 km segments over the cloud layers in the vicinity of the SHEBA site. Subsequently, vertical profiles were conducted $\sim$3–5 times per flight. Figure 6 shows two profiles of LWC (separated in time by about 1.5 hours) from the flight on July 18. It can be seen that there are substantial differences in LWC in some portions of the profiles, notably the layer between 4000 and 6000 m. The differences produce a discrepancy in LWP values on the order of 100 g m^{-2}. Although Arctic clouds often appear fairly uniform, they still display some degree of natural variability in time and space. Therefore we must ensure that the cloud layers observed by the microwave radiometers are well represented by the profile selected for validation.

[37] Flight patterns conducted between vertical ascents and descents generally consisted of straight and level segments through cloud layers at various altitudes. By calculating the mean LWC for

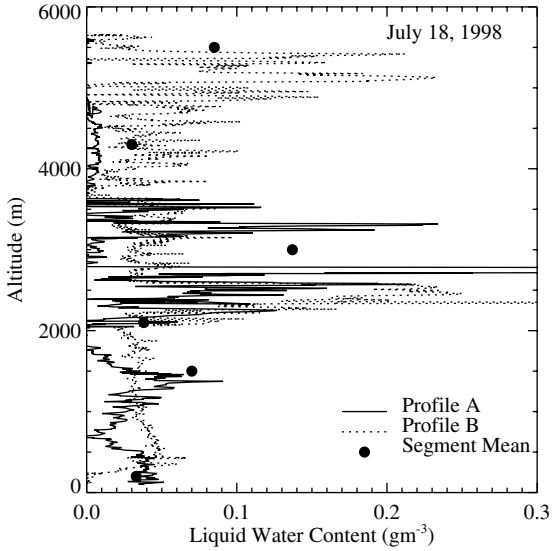

Figure 6. Vertical profiles of liquid water content near the SHEBA site as measured from the hot wire probe on the NCAR C-130 for two different times on July 18, 1998. Points represent means of liquid water content measured during straight and level flight segments through a cloud layer.

each of these straight and level segments, we can ascertain how well each profile represents the liquid water distribution over the observation area. In the example shown in Figure 6, mean LWC data from in-cloud segments at 200, 1500, 2100, 3000, 4300, and 5500 m are plotted along with two profiles that were fairly close in time to radiometer observations above the cloud. Except for the point at 1500, profile B appears to better represent the cloud layers observed. We note that the point at 4300 m matches neither profile very well, but the standard deviation of LWC during that segment was quite large, and profile B falls within one standard deviation of the mean at that level. In this way we assess the profiles from each flight and select the one that most closely represents the cloud field observed by the radiometer.

5. Results

5.1. LWP Retrievals

[38] We consider seven cases with clouds observed on flights during May and July 1998. Two cases with clear skies below the aircraft are also considered for purposes of validating the algorithm. Conditions compiled from flight reports and measurements from the cloud particle imager [*Jensen and Lawson*, 1999] are summarized in Table 3. The cases represent a range of cloud depths, liquid water contents, phase, and temperature.

[39] LWP estimates from the AIMR 90 GHz (horizontal polarization) channel are compared with LWP values derived from aircraft measurements of LWC. Since the aircraft slant profiles cover a significant horizontal distance, we cannot compare LWP at a single location. Therefore we calculate the mean LWP retrieved from AIMR over the extent of the observation area (typically 50 $\times$ 50 km centered on the SHEBA site) and compare it with the vertically integrated aircraft liquid water profile. The comparisons for all cases are shown in Figure 7. Among these cases, we see LWP values that range from near zero to 300 g m^{-2}. The correlation between mean retrieved LWP and in situ values is high (r = 0.989 with an RMS error of 14 g m^{-2}) although there is substantial variability in the retrieved values as shown by the vertical bars in Figure 7. Differences are largest at small values of LWP since uncertainties in surface emissivity have the largest influence at low liquid water amounts. As we move to higher

Table 3. Cloud Characteristics for Cases Used in LWP Retrievals

Case	Date	Cloud Levels, m	Cloud Type, Phase
1	May 15	150–650	stratus, predominantly liquid with some ice
2	May 18	100–450	homogeneous boundary layer cloud, supercooled water
3	May 20	clear	n/a
4	May 27	50–500, 1400–1600	low-level stratus, all liquid intermittent upper layer, liquid
5	July 8	5600–7100	cirrus, clear sky below
6	July 18	0–6000	multilayer, stratus, altostratus, and cirrus, layers of all ice, all liquid and mixed
7	July 26	0–6500 (variable)	layers of all ice, all liquid and mixed, periods of liquid and ice precipitation observed
8	July 27	2000–6300 (variable)	convective clouds, layers of all ice, all liquid and mixed phase
9	July 29	60–470, 1900–2130	homogeneous low-level stratus, upper layer dissipated during flight, all liquid

LWP values where surface influence is less apparent, the agreement between retrieved and in situ values improves. For example, the mean retrieved LWP is 88 g m^{-2} on July 28 with σ = 89 g m^{-2} and the in situ LWP is 84 g m^{-2}. The discrepancy is larger on July 26 (66 g m^{-2} versus 52 g m^{-2}); this may be partly due to inaccurate specification of the surface emissivity. On this day, intermittent precipitation was observed, so surface dielectric properties may have been modified by snowfall. Unfortunately, the low cloud base made it impossible to fly below the cloud, so it was not possible to revise our surface emissivity estimate with current data.

[40] In Figures 8 and 9 we consider two cases in more detail. Frequency distributions of retrieved LWP are plotted for each case,

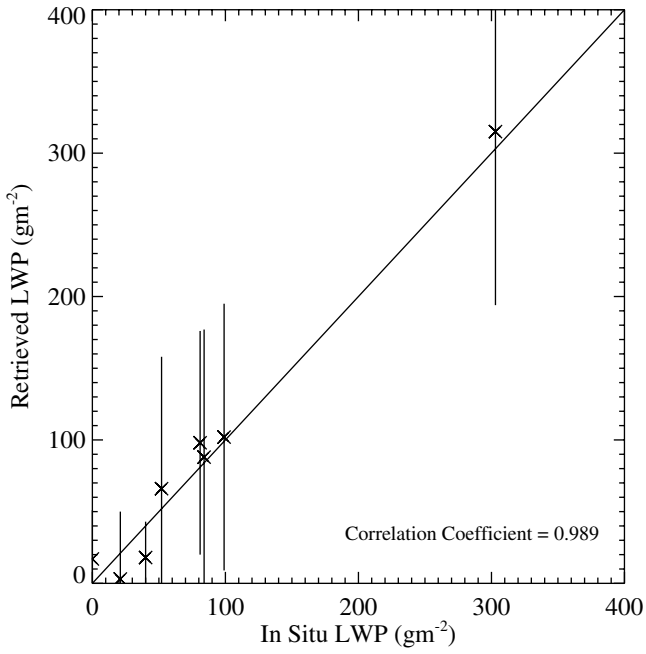

Figure 7. Comparison of mean LWP retrieved from passive microwave measurements with LWP calculated from in situ measurements of liquid water content along an aircraft slant profile.

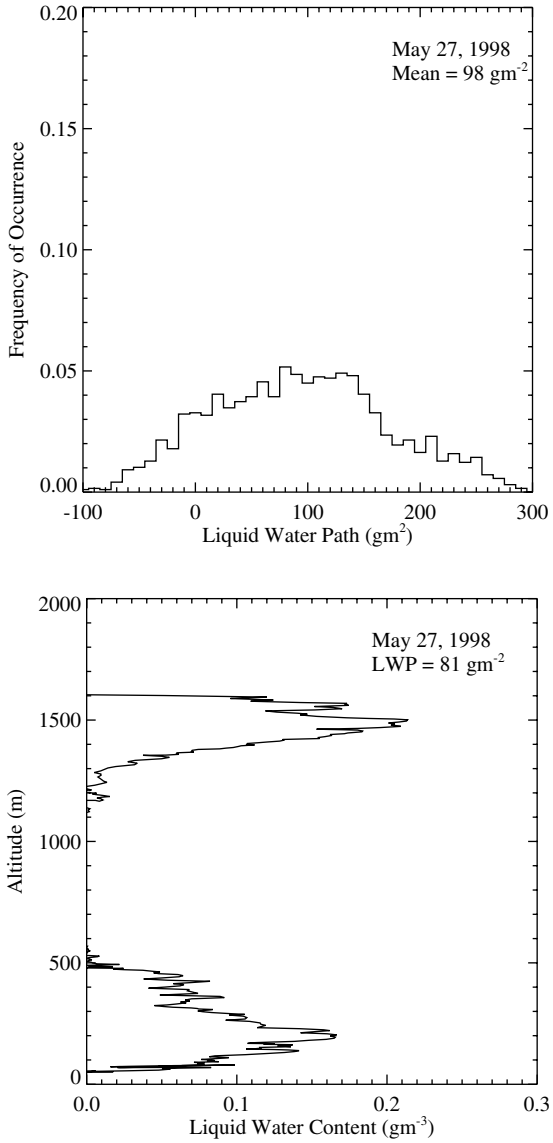

Figure 8. Distribution of retrieved LWP on May 27, 1998 (top figure) and aircraft liquid water content profile (bottom figure).

along with the corresponding LWC aircraft profile. On May 27 (Figure 8), relatively high levels of liquid water were measured in two cloud layers. At the in situ LWP of 81 g m^{-2}, model simulations suggest that the cloud-induced ΔT_B is on the order of 10–15 K, while surface emissivity uncertainties change T_B by about 5 K. In this situation we would expect the algorithm to have reasonable skill in estimating LWP. Although the mean retrieved value does overestimate the in situ value by about 18%, the agreement is reasonable considering the 15% uncertainty in the hot wire probe measurement. We note that May 27 exhibited changes in surface conditions as the snow began to melt, so the clear-sky surface emissivity value assumed for other dates in May was revised upward on the basis of below-cloud AIMR measurements taken on that day. On July 18 (Figure 9) a deep cloud layer produced the highest LWP values encountered during FIRE-SHEBA flights. For LWP, near 300 g m^{-2}, we see a relatively small influence on T_B from surface emission compared to liquid water emission. The agreement between mean retrieved and in situ LWP is very good in this case (315 g m^{-2} and 303 g m^{-2}, respectively).

[41] Liquid water path retrievals for clear-sky cases provide a quantitative estimate of the minimum uncertainty of the algorithm. We consider one clear-sky case (May 20) and a second case where no liquid water was present below the aircraft (July 8). Retrievals are performed to ascertain whether a bias exists and to determine how much scatter is present. The mean retrieved LWP for the two cases is 17 g m^{-2} with σ = 34 g m^{-2}. These results are consistent with uncertainties seen in low LWP cases.

[42] In summary, we obtained good agreement between mean retrieved LWP and in situ measurements when LWP values were high and when the surface emissivity was well specified. The skill appears to diminish at low LWP values and/or when we do not have good estimates of surface emissivity. The cases analyzed here suggest that 50–60 g m^{-2} may be a lower limit for detectability by this algorithm. Given this information, we can then address the question of how often the algorithm would be useful in the Arctic.

[43] Analyses of ground-based radar and lidar data [*Intrieri et al.*, 2001] indicate that clouds were present 85% of the time during the SHEBA year. Maximum cloudiness occurred in the summer (90%) with minimum values in the winter (70%). Lidar measurements indicate that liquid water was present throughout the year,

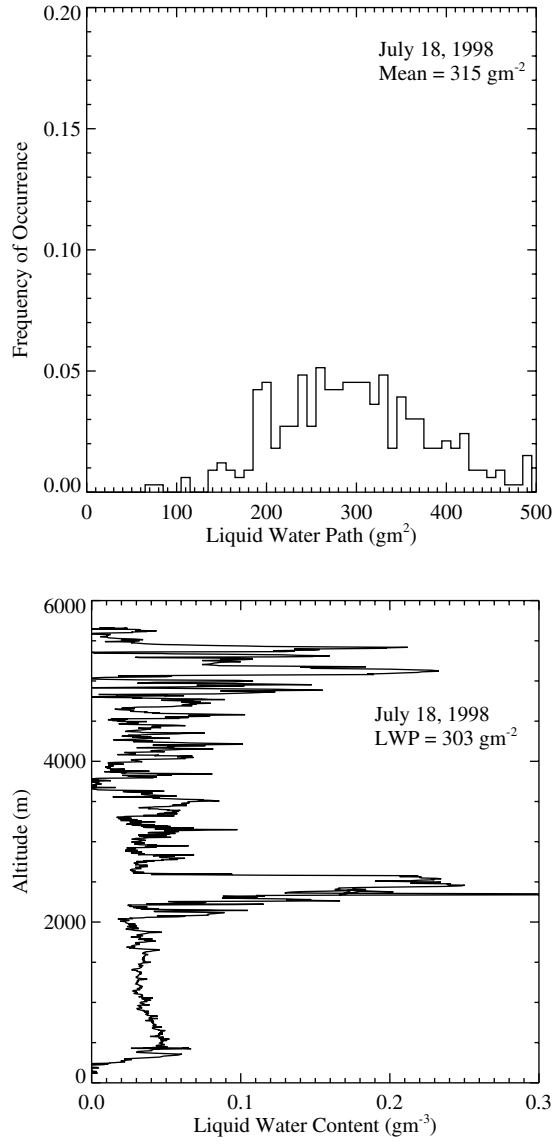

Figure 9. As in Figure 9 but for July 18, 1998.

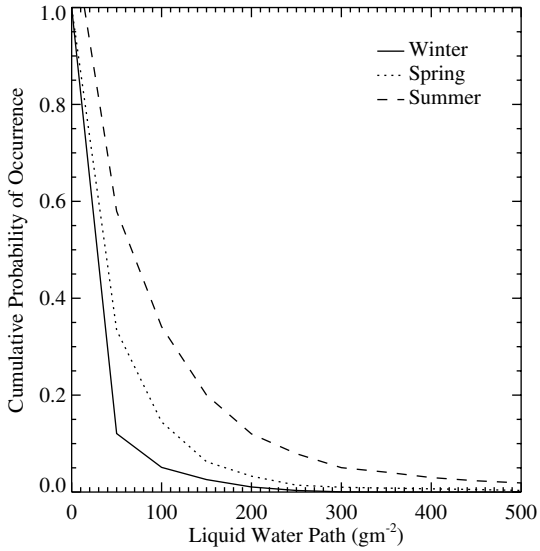

Figure 10. Cumulative probability of occurrence of LWP values at SHEBA as measured from the ground-based microwave radiometer.

even in the cold winter months. Specifically, liquid water was present in an average of 73% of the observed clouds. The ground-based microwave radiometer deployed at the SHEBA site measured LWP over 9 months of the SHEBA year. Figure 10 shows the frequency of occurrence of LWP larger than a given value for three seasons. Assuming levels of LWP detectable by this algorithm are 70 g m^{-2} and greater, we conclude that useful measurements could be obtained 10% of the time in winter, 28% of the time in spring, and 50% of the time in summer.

5.2. Cloud Detection Using Polarization Differences

[44] We have shown that low LWP values may be within noise limits of this algorithm and/or overwhelmed by uncertainty in the calculation of T_{B0}. In situations where LWP is below detectable thresholds or a reasonable estimate of surface emissivity is not available, it might be useful to simply know whether a liquid water cloud is present (for purposes of identifying clutter in sea ice classification schemes, for example) and to have some indication of whether the cloud contains large or small amounts of liquid water.

[45] Sea ice surfaces generally exhibit some degree of polarization at microwave frequencies. Tabulated values of horizontal and vertical emissivity at 90 GHz for various ice types show polarization differences of at least 0.03 [*Eppler et al.*, 1992]. Resulting horizontal and vertical components of brightness temperature will display differences of several degrees Kelvin. The radiation emitted and reflected by a polarized surface will depolarize as it passes through a liquid water cloud, thereby diminishing the difference between horizontal and vertical components of T_B. The degree of depolarization is related to the cloud LWP and the atmospheric water vapor burden. This phenomenon has been exploited by *Greenwald et al.* [1997] for retrievals of cloud LWP over land. Following their discussion, we define a normalized polarization difference (NPD) parameter as

$$NPD = \frac{T_{Bv} - T_{Bh}}{\varepsilon_{sv} - \varepsilon_{sh}},$$

where T_{Bv} and T_{Bh} are vertical and horizontal polarized components of the brightness temperature and ε_{sv} and ε_{sh} are the polarized components of surface emissivity. Normalizing the T_B polarization difference with the emissivity difference effectively removes the influence of varying surface polarization and provides us with a standardized parameter to assess depolarization due to atmospheric (cloud and water vapor) attenuation. Furthermore, NPD depends on differences rather than single values of T_B and ε_s; relative errors between the horizontal and the vertical components are presumably smaller than absolute errors in each measurement.

[46] NPD at 90 GHz has been calculated for the theoretical cases described in Table 2 and for the cases used for LWP retrievals described in Table 3. Results are shown in Figure 11. In both the theoretical and the actual cases we see that NPD decreases as LWP increases. We note the significant discrepancy between NPD at low LWP values for the theoretical cases and the retrieval cases. We believe this is a result of differences in water vapor. In the theoretical cases, only LWP was varied, while water vapor amounts were held constant. Therefore the water vapor levels are higher than in the retrieval cases, causing additional depolarization and lower NPD values. Since the retrieval cases are more physically realistic, the NPD values should be more indicative of the actual depolarization caused by atmospheric attenuation. On the basis of the data points representing the retrieval cases, we surmise that an NPD value above 200 K is a good indicator of very small LWP and would suggest that our retrieval algorithm would not perform very well. NPD below 100 K is probably a good indicator of high LWP. The intermediate range of 100–200 K corresponds to LWP of 50–100 g m^{-2}. While we are not attempting to relate NPD to a quantitative estimate of LWP, the information it provides might still be useful for screening purposes. We note, however, that depolarization can be attributed to other effects, such as new snow on the surface. Therefore even qualitative interpretation of the NPD value requires some information about possible changes to the surface emissivity difference.

5.3. Simulated Satellite Retrievals

[47] In considering the application of our LWP retrieval method to satellite-based sensors such as SSM/I, we must identify alternate sources for the ancillary information (T_S, T_C, T_A, and T_{B0}) obtained from aircraft measurements. Calculation of T_{B0} requires surface temperature, atmospheric profiles of temperature and humidity, and surface emissivity. Surface temperature estimates can be obtained from AVHRR-based algorithms in clear-sky conditions; methods

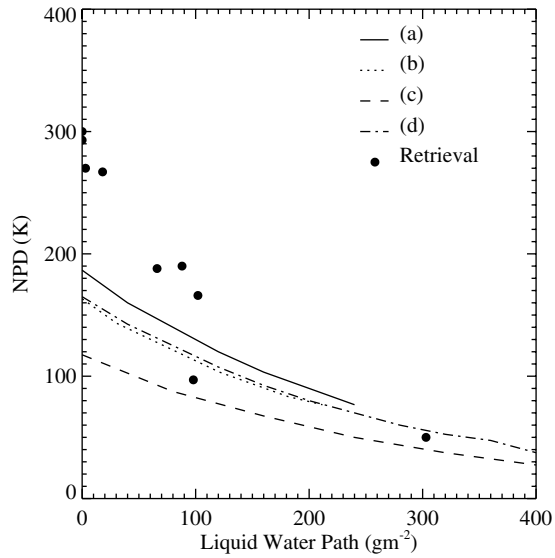

Figure 11. Modeled and retrieved values of the normalized polarization difference parameter. Cases a–d correspond to model simulations described in Tables 1 and 2.

for retrieving surface temperature in cloudy conditions are under development [*Key et al.*, 1997]. While the accuracy may not be so good as surface- or aircraft-based measurements, model simulations showed that the effect of errors in surface temperature on T_B (Figure 3) are less significant than effects of errors from other sources. Profiles of temperature and humidity can be compiled from the European Centre for Medium-Range Weather Forecasts (ECMWF) analyses and used to estimate T_C, T_A, and the atmospheric contribution to T_{B0}. Surface emissivity is probably the most difficult variable to estimate from satellite data. While the practice of using emissivity estimates from a recent clear-sky day can be applied for satellite retrievals as it was for the aircraft retrievals described here, verification of the accuracy of the estimate with below- cloud radiometer measurements is no longer possible. In addition, coarse spatial resolution (15 km at 85 GHz for SSM/I) makes the elimination of leads impossible, so the surface emissivity estimates and brightness temperature measurements will comprise different ice types. Finally, an automated method to identify precipitation using brightness temperature measurements would be desirable. Scattering indices such as those developed by *Grody* [1991] for use with SSM/I data or by *Bauer and Grody* [1995] for use with SSM/I and SSM/T2 data have been shown useful in separating snow cover and precipitation, although they have not been tested over sea ice.

[48] We examine the effects of degraded spatial resolution and larger uncertainties in surface emissivity estimates on LWP retrievals by performing a simulated satellite retrieval for four of the cases examined in previous sections. High-resolution brightness temperature measurements from aircraft are averaged over an area equivalent to an SSM/I pixel. Estimates of surface emissivity are revised to include leads previously excluded in our retrievals. Note that changes in emissivity with the inclusion of leads are fairly small since the lead fraction in May was on the order of 5%, while in July, open water features are often subpixel size even for the airborne sensors and were therefore included in the original estimate. Constant values of emissivity derived from clear-sky estimates are assumed for May and for July, despite information we have about changes in surface dielectric properties at specific times during these months.

[49] Table 4 compares mean retrieved LWP from the aircraft with that estimated by the simulated satellite retrievals using an areal averaged T_B. The cases on May 15 and July 18 show fairly small differences. On these days we know that the surface emissivity derived from nearby clear sky days was a good representation of the actual emissivity. The major difference then is the inclusion of leads in the retrievals and in the emissivity estimate. Given the small lead fractions, the effect is minimal, and resulting LWP estimates are similar for the aircraft retrievals and the simulated satellite retrievals. The situation is different in the other two cases (May 27 and July 29). Here we know that the surface emissivity estimates are less accurate, and the resulting LWP values deviate significantly from the aircraft LWP values. These cases confirm our earlier conclusion that good estimates of surface emissivity are critical for success of the retrieval algorithm. In cases where a good surface emissivity estimate is available the effects of degraded spatial resolution do not appear to be significant.

Table 4. Comparison of LWP Retrieved From Aircraft Data With LWP From Simulated Satellite Retrievals

Case	Date	LWP, g m $^{-2,}$	
		Aircraft	Simulated Satellite
1	May 15	3	11
3	May 27	98	209
4	July 18	315	355
7	July 29	102	197

6. Conclusions

[50] Model simulations of upwelling brightness temperature in Arctic conditions have been used to demonstrate that liquid water clouds over sea ice produce detectable increases in brightness temperature and that the magnitude of the increase is proportional to LWP. Brightness temperatures at 90 GHz show the largest response to LWP for the conditions considered when compared to responses at 37, 150, and 220 GHz. Sensitivity analyses were performed by varying surface and other atmospheric parameters that affect upwelling brightness temperature. Uncertainties in surface emissivity have the most significant influence on brightness temperature, especially at low values of LWP.

[51] An algorithm, developed for estimation of LWP over oceans using SSM/I data, has been adapted for use over sea ice with airborne microwave radiometer data. Ancillary data required as input is obtained from aircraft measurements. The algorithm has been applied to seven cases observed during the FIRE-SHEBA aircraft campaigns. Mean retrieved values of LWP have been compared to aircraft in situ measurements with mixed results. Agreement between the two data sets is very good at high LWP values (100 g m^{-2} and above). Discrepancies are largest at very low LWP (<50 g m^{-2}) where the magnitude of brightness temperature variations due to surface emissivity uncertainties is comparable to the cloud liquid water signal. Independent measurements of cloud properties during SHEBA demonstrate that clouds are present a high percentage of the time in the Arctic and that nearly three fourths of the clouds contain liquid water.

[52] In considering the extension of this method to satellite sensors we recognize that ancillary data such as rawinsonde profiles are not readily available in the Arctic. Use of the normalized polarization difference (NPD) is suggested as a method for qualitatively estimating LWP when insufficient ancillary data are available for the retrieval algorithm. We also note that surface emissivity estimates of sufficient accuracy are not easily obtained. In this work we were able to derive emissivity from cloud-free measurements relatively close in time to our cloud observations. Given the extensive cloudiness in the Arctic, representative clear-sky data may not always be available from a satellite platform. In such situations, knowledge of the ice type can give some indication of the proper emissivity value, but error bars are certainly larger. Given that retrievals are less sensitive to surface emissivity in conditions with high liquid water amounts, however, it may be possible to estimate LWP in those cases even with a crude estimate of surface emissivity.

[53] As asserted in previous theoretical and observational studies [*English*, 1999; *Combs et al.*, 1998; *Greenwald et al.*, 1997], this work confirms the hypothesis that passive microwave measurements provide information about the variation in cloud liquid water over nonwater surfaces. Furthermore, we have demonstrated by comparison with in situ LWP measurements that quantitative retrievals are possible in some situations. Although estimates of the liquid water amount in Arctic clouds may be available only a portion of the time using methods presented here, certain applications could still benefit from the limited information provided. Sea ice classification methods using SSM/I frequencies will be affected by cloud-induced T_B changes, so knowledge of the presence of a cloud and/or its contribution to the T_B signal could improve classification results [*Cavalieri et al.*, 1999]. Similarly, sea ice motion calculations that rely on SSM/I 85 GHz data [*Emery et al.*, 1997] will experience contamination from clouds and might therefore benefit from the capability to detect clouds. Global cloud data products (International Satellite Cloud Climatology Project (ISCCP)) currently show a low bias in cloud fraction over the poles [*Rossow and Schiffer*, 1999]. Current cloud detection methods used for assembling these products are based on visible and infrared

thresholds, so microwave retrievals of cloud liquid water path over sea ice might provide complimentary information about the presence of clouds.

[54] **Acknowledgments.** This research was supported by the NSF SHEBA program, the NASA FIRE program, and a NASA Earth System Science Fellowship. G. Liu's participation in this project was supported by NSF ATM-0002860.

References

Bauer, P., and N. C. Grody, The potential of combining SSM/I and SSM/T2 measurements to improve the identification of snow cover and precipitation, *IEEE Trans. Geosci. Remote Sens.*, *33*, 252–261, 1995.

Browning, K. A., Survey of perceived priority issues in the parameterizations of cloud-related processes in GCMs, *Q. J. R. Meteorol. Soc.*, *120*, 483–487, 1994.

Cavalieri, D. J., K. M. St. Germain, and C. T. Swift, Reduction of weather effects in the calculation of sea-ice concentration with the DMSP SSM/I, *J. Glaciol.*, *41*, 455–464, 1999.

Collins, M. J., F. G. R. Warren, and J. L. Paul, Airborne imaging microwave radiometer, part I, Radiometric analysis, *IEEE Trans. Geosci. Remote Sens.*, *34*(3), 643–655, 1996.

Combs, C. L., T. J. Greenwald, A. S. Jones, D. L. Randel, and T. H. Vonder Haar, Satellite detection of cloud liquid water over land using polarization differences at 85.5 GHz, *Geophys. Res. Lett.*, *25*, 75–78, 1998.

Curry, J. A., E. E. Ebert, and J. L. Schramm, Impact of clouds on the surface radiation balance of the Arctic Ocean, *Meteorol. Atmos. Phys.*, *51*, 197–217, 1993.

Curry, J. A., W. B. Rossow, D. Randall, and J. L. Schramm, Overview of arctic cloud and radiation characteristics, *J. Clim.*, *9*, 1731–1764, 1996.

Curry, J. A., et al., FIRE Arctic clouds experiment, *Bull. Am. Meteorol. Soc.*, *81*(1), 5–29, 2000.

Emery, W. J., C. W. Fowler, and J. A. Maslanik, Satellite-derived maps of Arctic and Antarctic sea ice motion: 1988-1994, *Geophys. Res. Lett.*, *48*, 11–64, 1997.

English, S. J., Estimation of temperature and humidity profile information from microwave radiances over different surface types, *J. Appl. Meteorol.*, *38*, 1526–1541, 1999.

English, S. J., and T. J. Hewison, A fast generic millimetre-wave emissivity model, *Proc. SPIE*, *3503*, 288–300, 1998.

Eppler, D. T., et al., Passive microwave signatures of sea ice, in *Microwave Remote Sensing of Sea Ice, Geophys. Monogr. Ser.*, vol. 68, edited by F. D. Carsey, 462 pp., AGU, Washington, D. C., 1992.

Evans, K. F., and G. L. Stephens, Microwave radiative transfer through clouds composed of realistically shaped ice crystals, part I, Single scattering properties, *J. Atmos. Sci.*, *52*, 2041–2057, 1995.

Francis, J. A., Cloud radiative forcing over arctic surfaces, in *Preprints of Fifth Conference on Polar Meteorology and Oceanography*, pp. 221–226, Am. Meteorol. Soc., Boston, Mass., 1999.

Gerber, H., B. G. Arends, and A. S. Ackerman, New microphysics sensor for aircraft use, *Atmos. Res.*, *37*, 235–252, 1994.

Greenwald, T. J., C. L. Combs, A. S. Jones, D. L. Randel, and T. H. Vonder Haar, Further developments in estimating cloud liquid water over land using microwave and infrared satellite measurements, *J. Appl. Meteorol.*, *36*(4), 389–405, 1997.

Grody, N. C., Classification of snow cover and precipitation using the Special Sensor Microwave Imager, *J. Geophys. Res.*, *96*, 7243–7435, 1991.

Grody, N. C., Remote sensing of the atmosphere from satellites using microwave radiometer, in *Atmospheric Remote Sensing by Microwave Radiometry*, edited by M. A. Janssen, 572 pp., John Wiley, New York, 1993.

Haggerty, J. A., Airborne passive microwave measurements of arctic clouds and sea ice, Ph.D. dissertation, Dep. of Aerosp. Eng. Sci., Univ. of Colo., Boulder, Colo., 2001.

Haggerty, J. A., and J. A. Curry, Variability of sea ice emissivity estimated from airborne passive microwave measurements during FIRE SHEBA, *J. Geophys. Res.*, *106*, 15,265–15,277, 2001.

Haggerty, J. A., et al., Heterogeneity of sea ice suface temperature at SHEBA from aircraft measurements, *J. Geophys. Res.*, in press, 2001.

Hollinger, J. P., B. E. Troy, R. O. Ramseier, K. W. Asmus, M. F. Hartman, and C. A. Luther, Microwave emission from high arctic sea ice during freeze-up, *J. Geophys. Res.*, *89*, 8104–8122, 1984.

Intrieri, J. M., M. D. Shupe, T. Uttal, and B. J. McCarty, Annual cycle of arctic cloud geometry and phase from radar and lidar at SHEBA, *J. Geophys. Res.*, in press, 2001.

Jensen, T. L., and R. P. Lawson, Observations in various cloud systems over the SHEBA ice station during FIRE-ACE, in *Proceedings of the Fifth Conference on Polar Meteorology and Oceanography*, pp. 150–154, Am. Meteorol. Soc., Boston, Mass., 1999.

Jones, A. S., and T. H. Vonder Haar, Retrieval of microwave surface emittance over land using coincident microwave and infrared satellite measurements, *J. Geophys. Res.*, *95*, 16,673–16,683, 1990.

Key, J. R., and R. G. Barry, Cloud cover analysis with AVHRR: Cloud detection, *J. Geophys. Res.*, *94*, 8521–8535, 1990.

Key, J. R., J. B. Collins, C. Fowler, and R. S. Stone, High-latitude surface temperature estimates from thermal satellite data, *Remote Sens. Environ.*, *61*, 302–309, 1997.

Khvorostyanov, V. I., J. A. Curry, J. O. Pinto, M. Shupe, and K. Sassen, Modeling with explicit spectral water and ice microphysics of a two-layer cloud system of altostratus and cirrus observed during the FIRE Arctic Clouds Experiment, *J. Geophys. Res.*, *106*, 15,099–15,112, 2001.

Kummerow, C., W. S. Olson, and L. Giglio, A simplified scheme for obtaining precipitation and vertical hydrometeor profiles from passive microwave sensors, *IEEE Trans. Geosci. Remote Sens.*, *34*, 1213–1232, 1996.

Liebe, H. J., and D. H. Layton, Millimeter wave properties of the atmosphere: Laboratory studies and propagation modeling, *NTIA Rep. 87-24*, 74 pp., Natl. Telecommun. and Inf. Admin., Washington, D. C., 1987.

Liebe, H. J., G. Hufford, and T. Manabe, A model for the complex permittivity of water at frequencies below 1 THz, *Int. J. Infrared Millimeter Waves*, *12*, 659–675, 1991.

Lin, B., P. Minnis, B. Wielicki, D. R. Doelling, R. Palikonda, D. F. Young, and T. Uttal, Estimation of water cloud properties from satellite microwave, infrared and visible measurements in oceanic environments, 2, Results, *J. Geophys. Res.*, *103*, 3887–3905, 1998.

Lin, B., P. Minnis, A. Fan, J. Curry, and H. Gerber, Comparison of cloud liquid water paths derived from in situ and microwave radiometer data taken during the SHEBA/FIRE ACE, *Geophys. Res. Lett.*, *28*, 975–978, 2001.

Lipton, A. E., M. K. Griffin, and A. G. Ling, Microwave transfer model differences in remote sensing of cloud liquid water at low temperatures, *IEEE Trans. Geosci. Remote Sens.*, *37*, 620–623, 1999.

Liu, G., A fast and accurate model for microwave radiance calculations, *J. Meteorol. Soc. Jpn.*, *76*(2), 335–343, 1998.

Liu, G., and J. A. Curry, Retrieval of characteristic features of cloud liquid water from satellite measurements, *J. Geophys. Res.*, *98*, 5069–5092, 1993.

Liu, G., and J. A. Curry, Remote sensing of ice water characteristics in tropical clouds using aircraft microwave measurements, *J. Appl. Meteorol.*, *37*, 337–355, 1998.

National Center for Atmospheric Research (NCAR) (Research Aviation Facility), The NCA/NSF EC-130Q Hercules (N130AR): Overview and summary of capabilities, *NCAR Tech. Bull.3*, Boulder, Colo., 1994.

Perovich, D. K., et al., Year on ice gives climate insights, *Eos Trans. AGU*, *80*(41), 481, 1999a.

Perovich, D. K., T. C. Grenfell, B. Light, J. A. Richter-Menge, M. Sturm, W. B. Tucker, III, H. Eichen, G. A. Maykut, and B. Elder, *Snow and Ice Studies*, [CD-ROM], U.S. Army Cold Reg. Res. and Eng. Lab., Hanover, N. H., 1999b.

Racette, P., R. F. Adler, and D. S. Zacharias, An airborne millimeter-wave imaging radiometer for cloud, precipitation, and atmospheric water vapor studies, *J. Atmos. Oceanic Technol.*, *13*, 610–619, 1996.

Ray, P. S., Braodband complex refractive indices of ice and water, *Appl. Opt.*, *11*, 1836–1844, 1972.

Rosenkranz, P., Water vapor microwave continuum absorption: A comparison of measurements and models, *Radio Sci.*, *33*, 919–928, 1998.

Rossow, W. B., and R. A. Schiffer, Advances in understanding clouds from ISCCP, *Bull. Am. Meteorol. Soc.*, *80*, 2261–2285, 1999.

Shupe, M. D., T. Uttal, S. Y. Matrosov, and A. S. Frisch, Cloud water contents and hydrometeor sizes during the FIRE Arctic Clouds Experiment, *J. Geophys. Res.*, *106*, 15,015–15,028, 2001.

Ulaby, F. T., R. K. Moore, and A. K. Fury, *Microwave remote sensing active and passive*, vol. 1, *Microwave Remote Sensing Fundamentals and Radiometry*, 456 pp., Artech House, Norwood, Mass., 1981.

Ulaby, F. T., R. K. Moore, and A. K. Fury, *Microwave Remote Sensing Active and Passive*, vol. III, *From Theory to Applications,* 2162 pp., Artech House, Norwood, Mass., 1986.

Wang, J. R., G. Liu, J. D. Spinhirne, P. Racette, and W. D. Hart, Observations and retrievals of cirrus cloud parameters using multichannel millimeter-wave radiometric measurements, *J. Geophys. Res.*, 106, 15,251–15,263, 2001.

Warren, S. G., Optical constants of ice from the ultraviolet to the microwave, *Appl. Opt.*, *23*, 1206–1225, 1984.

Washington, W. M., and G. A. Meehl, Climate sensitivity due to increased CO_2: Experiments with a coupled atmosphere and ocean general circulation model, *Clim. Dyn.*, *4*, 1–38, 1989.

Weng, F., and N. C. Grody, Retrieval of cloud liquid water using the special sensor microwave imager (SSM/I), *J. Geophys. Res.*, *99*, 25,535–25,551, 1994.

Westwater, E. R., Ground-based microwave remote sensing of meteorological variables, in *Atmospheric Remote Sensing by Microwave Radiometry*, edited by M. A. Janssen, 572 pp., John Wiley, New York, 1993.

Westwater, E. R., Y. Han, M. Shupe, and S. Y. Matrosov, Analysis of integrated cloud liquid and precipitable water vapor retrievals from microwave radiometers during the Surface Heat Budget of the Arctic Ocean project, *J. Geophys. Res.*, *106*, 32,019–32,030, 2001.

J. A. Curry, Program in Atmospheric and Oceanic Sciences, University of Colorado, Boulder, CO 80302, USA.

J. Haggerty, National Center for Atmospheric Research, P. O. Box 3000, Boulder, CO 80307, USA. (haggerty@ucar.edu)

G. Liu, Department of Meteorology, Florida State University, Tallahassee, FL 32306, USA.